Marangoni spreading and contracting three-component droplets on completely wetting surfaces

Dieter A. Baumgartner[a,b] , Samira Shiri[a,c] , Shayandev Sinha[a,1] , Stefan Karpitschka[d], and Nate J. Cira[a,c,2]

When a droplet comes in contact with a completely wetting surface, the liquid typically spreads until it covers the entire substrate. However, nonuniform evaporation of a multi-component droplet can generate surface tension gradients that alter this behavior. Here, we explore the rich dynamics of fully miscible, three-component droplets composed of water, ethanol, and propylene glycol on completely wetting glass substrates. These droplets initially spread rapidly but then stop and contract. We experimentally and theoretically investigate this behavior throughout the ternary parameter space at different relative humidities. Evaporation changes the composition of the droplet over space and time, resulting in a reversal of Marangoni flows that ultimately determines the dynamic droplet shape. We illustrate the utility of such dynamics by collecting, aggregating, and removing contaminants from a 4-cm² area using a single μL-scale droplet.

surface wetting | Marangoni stress | multicomponent droplet | surface cleaning | evaporating droplet

Liquid droplets interacting with solid surfaces are found in numerous applications, such as water (H_2O)-repellent coatings (1), paint, self-cleaning surfaces (2), heat transfer (3, 4), and pesticide treatment (5), and are the subject of intense fundamental research (6). On a fully wetting surface, a liquid droplet with a positive spreading parameter $S = \gamma_{sv} - (\gamma_{sl} + \gamma_{lv})$, with γ_{ij} the interfacial tensions between the solid (s), the liquid (l), and the vapor (v), will spread over the surface into a thin film, driven by capillarity. When a second component is present in the droplet, nonuniform evaporation and the resulting surface tension gradients can cause more complex dynamics. This may enhance spreading, popularly known from the "tears of wine" (7–10), utilized to efficiently cover large areas with a thin film of liquid (11). The opposite case, where the Marangoni flow is directed toward the bulk liquid, is known as "Marangoni contraction" and can even prevent droplets from spreading on completely wetting surfaces (10–14). Marangoni contraction can be used to cleanly remove liquids from high-energy surfaces (15).

Droplets with more than two components exhibit even more diverse behaviors that have been the center of various studies. For example, the evaporation of ouzo droplets, consisting of ethanol (EtOH), H_2O, and oil (16), generates surface tension gradients and precipitation of oil droplets, which collect around the droplet contact line. In whiskey (17), the combination of EtOH, H_2O, and surfactants generates surface tension-induced flows that can suppress the formation of ring stains (18) during drying. Other studies have investigated flower-like patterns with liquid-on-liquid spreading (19), Marangoni bursting with H_2O/EtOH on oil (20), or even evolution of complex droplet behaviors in automated multicomponent droplet-in-oil experiments (21). Spontaneous reversal from spreading to retraction has been observed as oil/surfactant mixtures become autophobic (22) or with N,N-dimethylformamide in humid environments (23).

Here, we investigate the dynamics of droplets that contain three fully miscible commonplace liquids on completely wetting substrates. Motivated by the negligible contact-line pinning for Marangoni-contracted binary droplets, even on rough or energetically heterogeneous surfaces (10–13), we chose to add a volatile spreading protagonist to a contracting mixture. Specifically, we dispensed droplets consisting of mixtures of H_2O, propylene glycol (PG), and EtOH on plasma-cleaned glass slides in a closed chamber with well-defined ambient humidity and temperature. We imaged the dynamics using shadowgraphy, background-oriented schlieren (BOS), and particle tracking. We additionally implemented a numerical lubrication model based on ref. 13 to gain access to variables that are hidden in the experiments and validate our mechanistic understanding of the experimental findings. Details on the methods are given in *SI Appendix*.

Results

Behaviors. We observed three primary behaviors within the ternary parameter space. First, some droplets continuously spread (Fig. 1*A*). This spreading is faster than Tanner's law (25), consistent with Marangoni flow of liquid away from the droplet's center

Significance

The shape and dynamics of small sessile droplets are dictated by capillary forces. For liquid mixtures, evaporation adds spatio-temporal modulation to these forces that can either enhance or inhibit droplet spreading, depending on the direction of the resulting Marangoni flow. This work experimentally and numerically demonstrates the coexistence of two antagonistic Marangoni flows in a ternary mixture. Played against each other, they can choreograph a boomerang-like wetting motion: Droplets initially rapidly spread, then contract into a compact cap shape. While such a behavior has been impossible in wetting scenarios of simple liquids, it enables spread–retract–remove surface processing with the addition of a single small liquid volume, demonstrated here in a surface-cleaning experiment.

[1] Present address: Technology Development Group, Intel Corporation, Hillsboro, OR 97124.

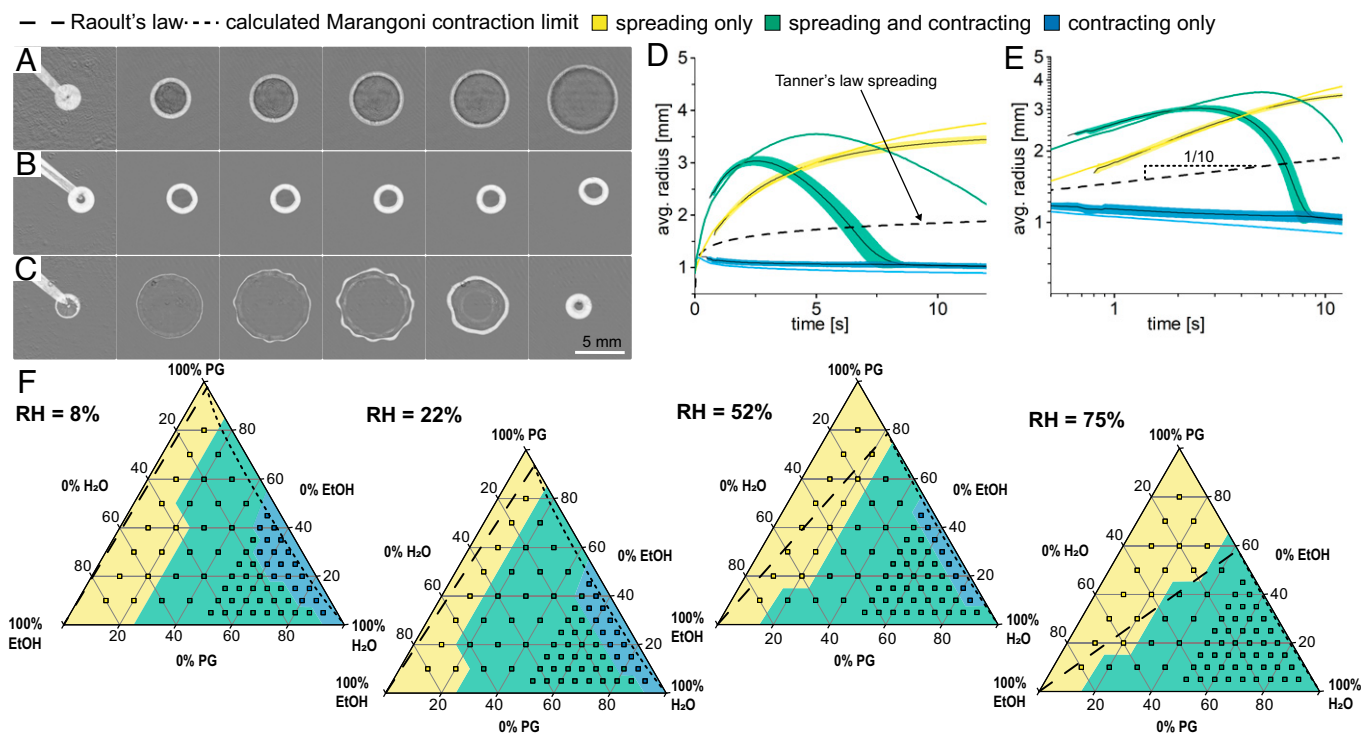[2] To whom correspondence may be addressed. Email: njc222@cornell.edu.

Fig. 1. Behaviors of ternary droplets on high-energy surfaces. (*A–C*) Time-series images ($t = 0, 1, 2, 3, 4$, and 10 s, at 52% RH, in V / V_{tot}, $V_{droplet} = 200$ nL) of (*A*) enhanced spreading 10% H_2O/70% PG/20% EtOH, (*B*) contracting 70% H_2O/25% PG/5% EtOH, and (*C*) spreading and contracting 50% H_2O/30% PG/20% EtOH. (*D* and *E*) Radius vs. time plots of the mixtures in *A–C* with *D* linear and *E* log axes ($n = 10$; SD shaded; solid colored lines correspond to the lubrication simulation). (*F*) The observable behaviors across the ternary parameter space at four different relative humidities. Overlaid are the theoretical considerations from Raoult's law (24) (dashed) and the net rate of change of the surface tension of the starting concentration (dotted). Avg., average.

(Fig. 1 *D* and *E*). Second, some droplets maintain a pseudo-steady radius and shape over time, consistent with Marangoni contraction (11–13) (Fig. 1 *B*, *D*, and *E*). Third, across a large portion of the ternary concentration space, we find droplets that first spread at an enhanced rate, then slow, stop, contract, and finally reach a pseudo-steady spherical cap-like state (Fig. 1 *C–E*). In these droplets, the apparent contact angle is variable around the droplet perimeter during expansion and increases throughout the behavior (see *SI Appendix*, Figs. S1 and S2 for contact-angle progressions overlaid with radii). The reduction in radius in the third case is due to the flow of liquid, rather than volume loss from evaporation. Our use of "contraction" follows from Marangoni-contracted droplets and describes the directional flow of liquid from the droplet edge to the center. While the first two behaviors are also exhibited by binary mixtures, the third behavior does not happen with droplets containing binary PG/H_2O, PG/EtOH, or H_2O/EtOH mixtures.

Mechanistic Understanding. Following what is known from previous work on the monotonic spreading (behavior 1) and Marangoni contraction (behavior 2) of two-component droplets, the two volatile components, EtOH and H_2O, are expected to exhibit antagonistic Marangoni forces when evaporating from a mixture with PG. EtOH evaporation promotes enhanced spreading, and H_2O evaporation promotes Marangoni contraction. We propose that the nonmonotonic droplet expansion and contraction (behavior 3) seen here is caused by a shifting balance between these two antagonistic forces due to a depletion of the most volatile component from the evaporating droplet.

Evaporation and the consequential depletion of volatile components is strongly nonuniform across such sessile droplets, with a sharp peak near the contact line when the droplet is flat (26, 27). EtOH, the most volatile component ($VP_{EtOH} = 5.8$ kPa), also

has the lowest surface tension ($\gamma_{EtOH} = 22$ mN · m^{-1}). Thus, initially, the dominant compositional change is a reduction of EtOH concentration close to the apparent contact line, which locally increases the surface tension. The resulting outward Marangoni stress enhances droplet spreading. On the other hand, evaporation of H_2O, the second most volatile component ($VP_{H_2O} = 2.3$ kPa) with the highest surface tension ($\gamma_{H_2O} = 72$ mN · m^{-1}), depletes H_2O in the vicinity of the apparent contact line, thereby decreasing the local surface tension. This causes an inward-facing Marangoni stress that counteracts the spreading motion. The evaporation of PG, which has a comparably low vapor pressure ($VP_{PG} = 17$ Pa, $\gamma_{PG} = 37$ mN · m^{-1}), is negligible as compared to the other components.

Thus, the overall dynamics are governed by the surface tensions of the components, ordered by their volatilities: The most volatile component (EtOH) evaporates fastest, generating initially strong, but also quickly decaying, Marangoni forces that cause the initial enhanced spreading, while the second most volatile component (H_2O) evaporates more slowly, leading to weaker, but more persistent, Marangoni forces that cause later contraction. However, the detailed spatiotemporal balance is more complex, with a coexistence of both effects during much of the process.

Varying Humidity. Evaporation rates are not only governed by the saturation vapor pressure of the pure components, but are strongly influenced by the concentrations of each component in the droplet and the gaseous environment. Far below the boiling point, evaporation is rate-limited by diffusion in the ambient air, so that the total evaporation rate of component i scales as

$$J_i \sim D_i \cdot (\overline{a}_i \cdot C_{sat,i} - C_{\infty,i}), \qquad [1]$$

with D_i the diffusion coefficient in air, $\overline{a}_i$ the activity in the liquid, $C_{sat,i}$ the saturated vapor concentration of the pure component,

and $C_{\infty,i}$ the ambient vapor concentration of component i. The second term is Raoult's law, where, for ideal mixtures, $\overline{a_i} = \chi_i$, the molar fraction. Changes to the composition of the mixture will change the liquid–vapor equilibrium and thus increase or decrease the evaporation rate, and departures from ideality and differences in diffusivities can play a role in dynamics, as recently emphasized for H_2O/alcohol mixtures (28).

To test our mechanistic understanding, we varied the ambient vapor concentration of H_2O C_{∞,H_2O} by changing the relative humidity (RH) and observed the droplet behavior across the ternary compositional space (Fig. 1F). In the high-PG/low-H_2O region, we found droplets that did not contract (Fig. 1 F, yellow region). The size of this region grows with increasing RH. This is consistent with Eq. 1: For $C_{\infty,H_2O} \geq \chi_{H_2O} \cdot C_{sat,H_2O}$, H_2O will not evaporate, and there is no driving force for droplet contraction. The dashed line [Raoult's law (24)] in Fig. 1F shows this transition, assuming an ideal mixture. Consistent with slower H_2O evaporation causing weaker contraction, we also found that at higher RH, droplets spread for a longer time and to larger maximum radii (*SI Appendix*, Fig. S3).

While the Raoult's law arguments establish the final fate of the droplet, to obtain an estimate for the initial contact-line motion, one must take into account that EtOH and H_2O are simultaneously evaporating over most of the parameter space. Thus, we calculate the initial net rate of change of surface tension due to evaporation as:

$$\frac{d\gamma_{net}}{dt} = J_{H_2O} \cdot \frac{d\gamma}{dC_{H_2O}} + J_{EtOH} \cdot \frac{d\gamma}{dC_{EtOH}}, \qquad [2]$$

with J_i from Eq. 1 and $\frac{d\gamma}{dC_i}$ the sensitivity of the surface tension to the respective component. Since evaporation and compositional changes are fastest near the contact line, $\frac{d\gamma_{net}}{dt} < 0$ and $\frac{d\gamma_{net}}{dt} > 0$ correspond to inward- and outward-pointing Marangoni flows, dominated by H_2O or EtOH loss, respectively.

By assuming ideal mixtures and estimating surface tensions by a linear interpolation of known values for binary mixtures, we found a region in the parameter space where the initial expansion should be fully suppressed (Fig. 1 F, dotted line). The observed dynamics show qualitative agreement with these considerations, with the "contraction-only" region occurring at low EtOH concentration

and low RH (Fig. 1 F, blue region). Quantitative deviations are expected, because the initial droplet deposition alters and obscures the very first moments of droplet spreading.

However, the actual spatiotemporal evolution of the droplet shape is even more complex because the nonuniform evaporation rates rapidly render the droplet composition spatially inhomogeneous, and the relevant physical effects are coupled to one another.

Lubrication Model. To obtain more detailed quantitative predictions, we implemented a lubrication model based on ref. 13, incorporating the effects of capillarity (Laplace and disjoining pressures), Marangoni flows, diffusion, and evaporation on an axisymmetric domain. Gravity, inertia, and thermal gradients are neglected. For details, see *SI Appendix*. This model reproduces the spreading and contraction dynamics (Fig. 1 D and E, solid colored lines) almost quantitatively. The remaining deviations are prominent only for the intermediate cases, in which the fine balance of Marangoni forces strongly depends on material parameters like surface tension and diffusivities. Importantly, we did not perform any parameter fitting, but relied directly on literature values available for the binary mixtures, extrapolating these nonlinear edges linearly into the ternary compositional space, where necessary.

In the model, both flow velocities and local compositions are readily available. For droplets with nonmonotonic spreading behavior, the model predicts a coexistence of the antagonistic Marangoni flows, long before and after the spreading reversal; the inner region is dominated by an outward Marangoni flow, mainly due to EtOH evaporation, and the outer region, where EtOH has depleted already, is dominated by an inward Marangoni flow. In both regions, two corresponding compensatory capillary flows (each in the direction opposite the two Marangoni flows) lead to the formation of two convection rolls (Fig. 2F, Movie S2, and *SI Appendix*, Fig. S4). As EtOH depletion continues, the outer region increases in size until it comprises the entire droplet. The apparent contact-line motion follows from a tug-of-war between these two regions.

Particle Tracking and BOS. To experimentally validate this finding, we imaged specific mixtures using a BOS setup and particle tracking (*SI Appendix*, *Methods*). BOS imaging revealed the
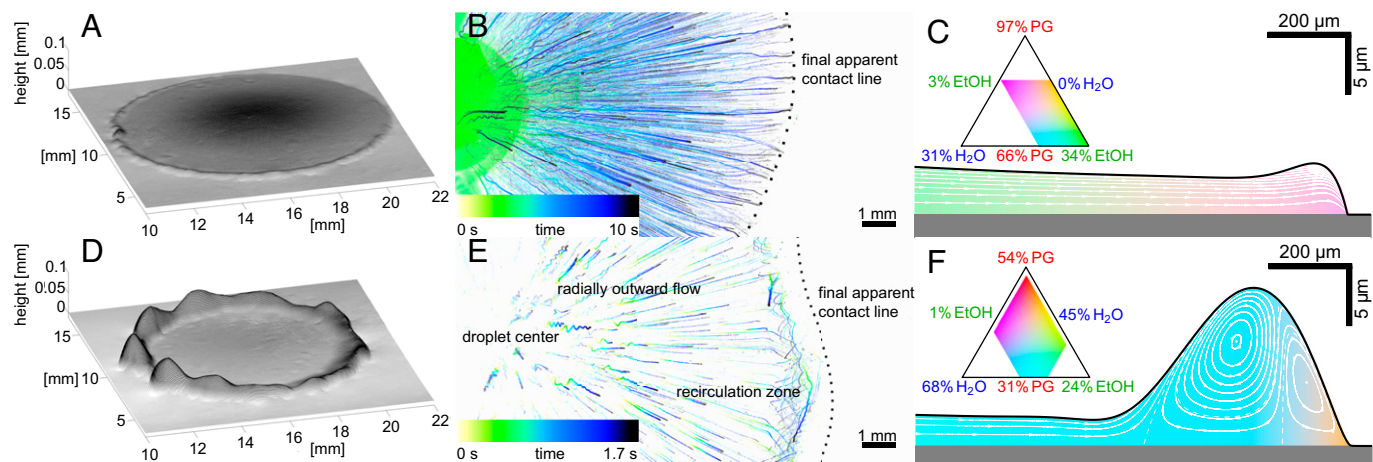

Fig. 2. Comparison between a binary droplet (A–C; 66% PG/34% EtOH at 52% RH) and a ternary droplet (D–F; 50% H_2O/35% PG/15% EtOH at 52% RH). Simulation data (C and F) are computed at 50% RH. (A) BOS reconstruction of the binary droplet shows a ridge of minimal height during spreading. (B) Particles move outward for the spreading binary droplet. (C) Lubrication model (66% PG/34% EtOH at 50% RH): PG enriches near the contact line (indicated by color code); all streamlines point outward (white lines). H_2O content stems from condensation on the droplet. (D) BOS reconstruction of the ternary droplet shows a prominent ridge during spreading. (E) During spreading, particles move outward at the center of the ternary droplet, but recirculate before reaching the edge. (F) Lubrication model (52% H_2O/32% PG/16% EtOH at 50% RH) around spreading reversal: Competing Marangoni flows collect liquid in a ridge, leading to counterrotating convection rolls. See also *SI Appendix*, Fig. S4 and Movie S2.
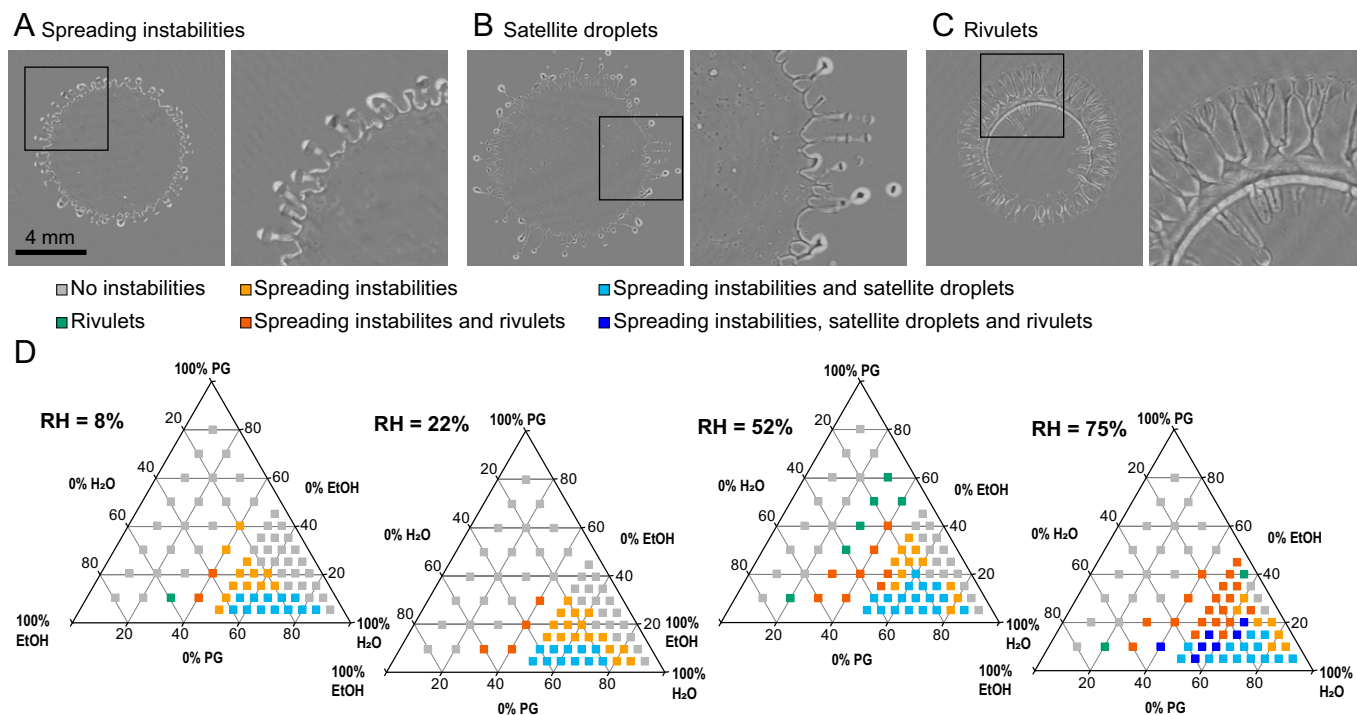
Fig. 3. Different forms of instabilities arising in ternary droplets. (*A*) Spreading instabilities of a droplet of 50% H_2O/20% PG/30% EtOH at 52% RH. (*B*) Vigorous instabilities with chaotic satellite droplet formation of a droplet of 50% H_2O/5% PG/45% EtOH at 44% RH. (*C*) Rivulet formation during the contracting phase of a droplet of 30% H_2O/10% PG/60% EtOH at 22% RH. (*D*) Observed instability formation across the ternary phase space at different humidities. Time lapses of *A–C* are shown in *SI Appendix*, Fig. S5 and Movie S4. $V_{droplet}$ = 200 nL for *A* and *C* and 100 nL for *B*, respectively.

development of a prominent ridge during expansion (Fig. 2*D*), much taller than that observed in enhanced binary spreading (Fig. 2*A*), consistent with collection of liquid due to opposing flows predicted by the model. Particle tracking also revealed a radial outward flow and an inner recirculation zone predicted by the model. Depletion of tracer particles from the outermost edge (Fig. 2*E*) during the dynamics made it difficult to see the predicted outer recirculation zone, but contraction of the droplet is strong evidence of an inward Marangoni flow from the droplet's edge. Eventually, the stagnation point along the liquid/vapor interface moves inward, reaching the center when the droplet is in the fully contracted state (Movie S3). This is different from the binary spreading case, in which particles move only radially outward. In both cases, wavy particle trajectories can be seen close to the droplet center, which may be Bénard–Marangoni instabilities that are smeared outward during droplet spreading (Fig. 2 *B* and *E*).

Instabilities. For many compositions, we observe that the droplet does not remain radially uniform throughout its life cycle (Fig. 3, *SI Appendix*, Fig. S5, and Movie S4). During expansion, fingering instabilities can emerge (Fig. 3*A*). Though visually reminiscent of crown formation in splashing droplets (29), they have origins related to Marangoni spreading instabilities previously reported for volatile binary droplets and single components on thermal gradients (30–32). The mechanism that was proposed to create this instability involves outward Marangoni flow causing a ridge to develop at the spreading front. Then, above a certain curvature, this ridge destabilizes into a series of periodic bulges that eventually develop into fingers (33).

Unlike previous cases, here the instabilities coarsen over time with an increasing wavelength as the Marangoni flow direction inverts until they eventually disappear completely (see *SI Appendix*, Fig. S1 for the contact-angle progression). Likely

due to complex spatiotemporal surface tension gradients, these instabilities can even detach from the parent droplet and form smaller satellite droplets that interact with each other (Fig. 3*B*) and the parent droplet. Low PG concentration produces more chaotic patterns and satellite droplets (Fig. 3*D*).

During contraction, some droplets leave behind cascading fractal-like drainage rivulets (Fig. 3*C*, *SI Appendix*, Fig. S5, and Movie S4). These are more prominent at high humidities or low H_2O concentration, suggesting a role for weaker inward Marangoni flow due to decreased H_2O evaporation (Fig. 3*D*). They are reminiscent of Saffman–Taylor-type patterns that can form with a lifted Hele–Shaw cell (see, for example, images in ref. 34); however, here, there is no second plate. These patterns also bear some resemblance to fractal-like patterns that can emerge during spreading on a liquid film (35), but they form during contraction, rather than spreading. The detailed mechanistic origin of the contracting pattern seen for some compositions here remains to be determined. Neither the spreading instabilities nor the contracting features are captured in the axisymmetric numerical simulation and warrant further investigation with analysis accounting for more than one dimension.

Discussion

Understanding the boomerang-like wetting motion of such multicomponent droplets enables control of autonomous, multistep, surface-processing technologies, such as the self-organized cleaning of a high-energy surface (Fig. 4). Liquids adhere strongly to high-energy surfaces, and removing them is nontrivial, but essential, to do cleanly in surface-sensitive processes, such as semiconductor manufacturing. Removal of liquid by evaporation is not effective since evaporation of residual liquids inevitably deposits solutes that contaminate the surface and impair contact-line mobility (18). Such deposition can be avoided by
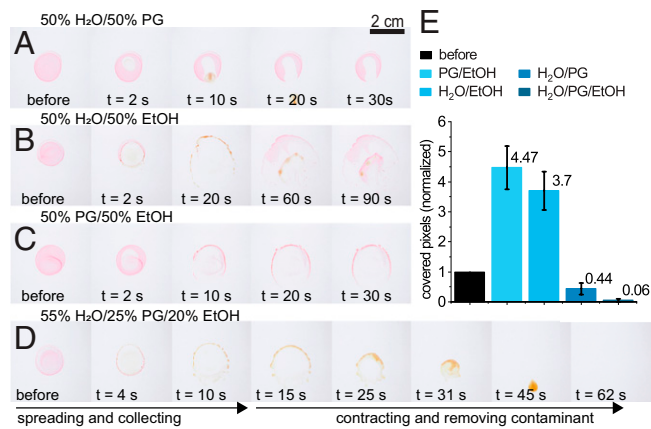
Fig. 4. Cleaning ability of binary and ternary mixtures. (*A–C*) All binary mixtures show poor cleaning ability. The contracting droplet in *A* only cleans a small part where it sits, while the droplets in *B* and *C* spread the contamination across the surface. (*D*) A ternary droplet has the ability to spread and dissolve the contaminant and then contract and collect all the debris within the droplet, before rolling off on an angle. See Movie S5. Downward migration results from a deliberately tilted slide. (*E*) Normalized visible contamination before and after cleaning with different mixtures (*n* = 10), errors bars indicate standard deviation.

removing the liquid from the surface with flow rather than evaporation. The time associated with spreading or drainage of a thin liquid film scales more favorably with film height, h, for shear stress-driven flows, such as Marangoni flows, than for pressure-driven flows ($1/h^2$ vs. $1/h^3$). Thus, Marangoni drying (15) is routinely utilized to remove liquids from silicon wafers after applying excess amounts of a processing fluid, e.g., during spinning or in a bath.

In Fig. 4, a dried contaminant (red) is removed completely by a ternary droplet (*D*), while any binary combination of the same three liquids either partially removes (*A*) or merely relocates (*B* and *C*) the contaminant (Movie S5). The unique expansion-then-contraction behavior of these ternary droplets combines the ability of Marangoni flows to first spread small amounts of a liquid over large areas and later drain them again cleanly, enabling a self-organized spread–react–remove-type surface processing.

More generally, we revealed how three-component droplets can dramatically change shape while evaporating on high-energy surfaces. The dominant shape changes are driven by the nonuniform evaporation of the different components at different rates, which spatio-temporally modulates surface tension gradients and the corresponding Marangoni flows. Depending on the surrounding vapor phase and the initial composition, the choreography of these flows can be controlled, allowing a tunable self-organized sequence of expansion and contraction with a complex internal flow structure. Cleaning with minimal liquid volume is just one of many possible uses for control of the location and duration of liquid exposure to the substrate.

Author affiliations: [a]Rowland Institute, Harvard University, Cambridge, MA 02142; [b]Environmental Microfluidics Group, Institute of Environmental Engineering, Department of Civil, Environmental, and Geomatic Engineering, ETH Zürich, 8093 Zürich, Switzerland; [c]Department of Biomedical Engineering, Cornell University, Ithaca, NY 14850; and [d]Max Planck Institute for Dynamics and Self-Organization, 37077 Göttingen, Germany

1. R. N. Wenzel, Resistance of solid surfaces to wetting by water. *Ind. Eng. Chem.* **28**, 988–994 (1936).
2. X. Zhang, F. Shi, J. Niu, Y. Jiang, Z. Wang, Superhydrophobic surfaces: From structural control to functional application. *J. Mater. Chem.* **18**, 621–633 (2008).
3. S. Daniel, M. K. Chaudhury, J. C. Chen, Fast drop movements resulting from the phase change on a gradient surface. *Science* **291**, 633–636 (2001).
4. S. Shiri, J. C. Bird, Heat exchange between a bouncing drop and a superhydrophobic substrate. *Proc. Natl. Acad. Sci. U.S.A.* **114**, 6930–6935 (2017).
5. M. C. Butler Ellis, C. R. Tuck, P. C. Miller, How surface tension of surfactant solutions influences the characteristics of sprays produced by hydraulic nozzles used for pesticide application. *Colloids Surf. A Physicochem. Eng. Asp.* **180**, 267–276 (2001).
6. D. Lohse, X. Zhang, Physicochemical hydrodynamics of droplets out of equilibrium. *Nat. Rev. Phys.* **2**, 426–443 (2020).
7. J. Thomson, On certain curious motions observable at the surfaces of wine and other alcoholic liquors. *Lond. Edinb. Dublin Philos. Mag. J. Sci.* **10**, 330–333 (1855).
8. C. Marangoni, Ueber die ausbreitung der tropfen einer flüssigkeit auf der oberfläche einer anderen. *Ann. Phys.* **219**, 337–354 (1871).
9. J. W. Gibbs, On the equilibrium of heterogeneous substances Part II. *Trans. Connecticut Acad. Arts Sci.* **3**, X (1878).
10. R. L. Cottington, C. M. Murphy, C. R. Singleterry, "Effect of polar-nonpolar additives on oil spreading on solids, with applications to nonspreading oils" in *Contact Angle, Wettability, and Adhesion*, F. M. Fowkes, Ed. (Advances in Chemistry, ACS Publications, Washington, DC, 1964), vol. 43, pp. 341–354.
11. W. D. Bascom, R. L. Cottington, C. R. Singleterry, "Dynamic surface phenomena in the spontaneous spreading of oils on solids" in *Contact Angle, Wettability, and Adhesion*, F. M. Fowkes, Ed. (Advances in Chemistry, ACS Publications, Washington, DC, 1964), vol. 43, pp. 355–379.
12. N. J. Cira, A. Benusiglio, M. Prakash, Vapour-mediated sensing and motility in two-component droplets. *Nature* **519**, 446–450 (2015).
13. S. Karpitschka, F. Liebig, H. Riegler, Marangoni contraction of evaporating sessile droplets of binary mixtures. *Langmuir* **33**, 4682–4687 (2017).
14. M. A. Hack *et al.*, Wetting of two-component drops: Marangoni contraction versus autophobing. *Langmuir* **37**, 3605–3611 (2021).
15. A. F. M. Leenaars, J. A. M. Huethorst, J. J. Van Oekel, Marangoni drying: A new extremely clean drying process. *Langmuir* **6**, 1701–1703 (1990).
16. H. Tan *et al.*, Evaporation-triggered microdroplet nucleation and the four life phases of an evaporating Ouzo drop. *Proc. Natl. Acad. Sci. U.S.A.* **113**, 8642–8647 (2016).
17. H. Kim *et al.*, Controlled uniform coating from the interplay of Marangoni flows and surface-adsorbed macromolecules. *Phys. Rev. Lett.* **116**, 124501 (2016).
18. R. D. Deegan *et al.*, Capillary flow as the cause of ring stains from dried liquid drops. *Nature* **389**, 827–829 (1997).
19. F. Wodlei, J. Sebilleau, J. Magnaudet, V. Pimienta, Marangoni-driven flower-like patterning of an evaporating drop spreading on a liquid substrate. *Nat. Commun.* **9**, 820 (2018).
20. L. Keiser, H. Bense, P. Colinet, J. Bico, E. Reyssat, Marangoni bursting: Evaporation-induced emulsification of binary mixtures on a liquid layer. *Phys. Rev. Lett.* **118**, 074504 (2017).
21. J. M. P. Gutierrez, T. Hinkley, J. W. Taylor, K. Yanev, L. Cronin, Evolution of oil droplets in a chemorobotic platform. *Nat. Commun.* **5**, 5571 (2014).
22. R. Tadmor *et al.*, Drops that change their mind: Spontaneous reversal from spreading to retraction. *Langmuir* **35**, 15734–15738 (2019).
23. S. W. Hu, C. Y. Wang, Y. J. Sheng, H. K. Tsao, Peculiar wetting of *N,N*-dimethylformamide: Expansion, contraction, and self-running. *J. Phys. Chem. C* **123**, 24477–24486 (2019).
24. F. M. Raoult, Loi générale des tensions de vapeur des dissolvants. *C. R. Hebd. Seances Acad. Sci.* **104**, 1430–1433 (1887).
25. L. H. Tanner, The spreading of silicone oil drops on horizontal surfaces. *J. Phys. D Appl. Phys.* **12**, 1473 (1979).
26. Y. O. Popov, Evaporative deposition patterns: Spatial dimensions of the deposit. *Phys. Rev. E Stat. Nonlin. Soft Matter Phys.* **71** (3 Pt 2B), 036313 (2005).
27. H. Hu, R. G. Larson, Evaporation of a sessile droplet on a substrate. *J. Phys. Chem. B* **106**, 1334–1344 (2002).
28. S. K. Parimalanathan, S. Dehaeck, A. Rednikov, P. Colinet, Controlling the wetting and evaporation dynamics of non-ideal volatile binary solutions. *J. Colloid Interface Sci.* **592**, 319–328 (2021).
29. R. D. Deegan, P. Brunet, J. Eggers, Complexities of splashing. *Nonlinearity* **21**, C1 (2008).
30. S. M. Troian, E. Herbolzheimer, S. A. Safran, J. F. Joanny, Fingering instability of driven spreading films. *Europhys. Lett.* **10**, 25–30 (1989).
31. S. M. Troian, X. L. Wu, S. A. Safran, Fingering instability in thin wetting films. *Phys. Rev. Lett.* **62**, 1496–1499 (1989).
32. A. P. Mouat, C. E. Wood, J. E. Pye, J. C. Burton, Tuning contact line dynamics and deposition patterns in volatile liquid mixtures. *Phys. Rev. Lett.* **124**, 064502 (2020).
33. A. M. Cazabat, F. Heslot, S. M. Troian, P. Carles, Fingering instability of thin spreading. *Nature* **245**, 118–143 (1990).
34. S. K. Thamida, P. V. Takhistov, H. C. Chang, Fractal dewetting of a viscous adhesive film between separating parallel plates. *Phys. Fluids* **13**, 2190–2200 (2001).
35. O. K. Matar, S. M. Troian, Spreading of a surfactant monolayer on a thin liquid film: Onset and evolution of digitated structures. *Chaos* **9**, 141–153 (1999).